Published in final edited form as:
*IEEE Trans Ultrason Ferroelectr Freq Control*. 2012 May ; 59(5): 893–904. doi:10.1109/TUFFC.2012.2274

# Quantitative Ultrasonic Characterization of Diffuse Scatterers in the Presence of Structures That Produce Coherent Echoes

**Adam C. Luchies [Student Member, IEEE]**, **Goutam Ghoshal**, **William D. O'Brien Jr. [Life Fellow, IEEE]**, and **Michael L. Oelze [Senior Member, IEEE]**
Department of Electrical and Computer Engineering, University of Illinois at Urbana-Champaign, Urbana, IL

Adam C. Luchies: luchies1@illinois.edu

## Abstract

Quantitative ultrasound (QUS) techniques that parameterize the backscattered power spectrum have demonstrated significant promise for ultrasonic tissue characterization. Some QUS parameters, such as the effective scatterer diameter (ESD), require the assumption that the examined medium contains uniform diffuse scatterers. Structures that invalidate this assumption can significantly affect the estimated QUS parameters and decrease performance when classifying disease. In this work, a method was developed to reduce the effects of echoes that invalidate the assumption of diffuse scattering. To accomplish this task, backscattered signal sections containing non-diffuse echoes were identified and removed from the QUS analysis. Parameters estimated from the generalized spectrum (GS) and the Rayleigh SNR parameter were compared for detecting data blocks with non-diffuse echoes. Simulations and experiments were used to evaluate the effectiveness of the method. Experiments consisted of estimating QUS parameters from spontaneous fibroadenomas in rats and from beef liver samples. Results indicated that the method was able to significantly reduce or eliminate the effects of non-diffuse echoes that might exist in the backscattered signal. For example, the average reduction in the relative standard deviation of ESD estimates from simulation, rat fibroadenomas, and beef liver samples were 13%, 30%, and 51%, respectively. The Rayleigh SNR parameter performed best at detecting non-diffuse echoes for the purpose of removing and reducing ESD bias and variance. The method provides a means to improve the diagnostic capabilities of QUS techniques by allowing separate analysis of diffuse and non-diffuse scatterers.

## I. Introduction

Quantitative ultrasound (QUS) parameters that provide information about tissue microstructure from the frequency content of ultrasonic backscattered signals have confirmed capabilities for ultrasonic tissue characterization [1]–[3]. For example, studies have used QUS parameters to successfully classify ocular lesions [4], prostate [5], liver disease [6], and tumors in rodent models of breast cancer [7]. QUS parameter estimation based on spectral analysis requires the assumption that incoherent scattering dominates the estimated backscattered power spectrum. This condition is satisfied when the interrogated medium can be modeled as a background medium with a large number of randomly spaced scatterers per resolution cell [2]. To estimate spectral-based QUS parameters, a parametric scattering model that describes the frequency response of a single radiating scatterer is fitted to the estimated power spectrum. The QUS parameter of interest in this work is the effective scatterer diameter (ESD), which captures information about the size of the modeled scatterers.

Biological tissues often contain complex structures that invalidate the assumption of the diffuse scatterer model necessary for many QUS parameter estimation techniques.

Therefore, tissue models have been proposed to include the existence of a more complex collection of scatterers [8]–[10]. For example, scatterers might be organized into different components. The first component, known as the diffuse component, consists of the described collection of diffuse scatterers, where many scatterers exist in each resolution cell and are also randomly positioned spatially [10]. The second component, known as the coherent component, consists of non-randomly spaced scatterers with some degree of organization and that produce resolvable echoes [10]. The coherent component can be further divided into long-range and short-range order, if desired, to produce a three-component model [8], [9]. Long-range order consists of periodically (nonrandomly) spaced scatterers, where the periodic spacing exists throughout the tissue region. Short-range order consists of nonrandomly spaced scatterers such as blood vessels or organ boundaries that produce strong echoes (i.e., specular scatterers).

The estimated backscattered power spectrum will include incoherent and coherent parts [11]. When the medium is accurately modeled as a single-component collection of diffuse scatterers, the coherent part of the spectrum acts as noise compared with the incoherent part of the spectrum. In contrast, when a two- or three- component model more accurately describes the medium (i.e., periodic or specular scatterers exist in the medium), the incoherent part of the spectrum no longer dominates and the coherent part of the spectrum can significantly affect the shape of the estimated power spectrum.

Scatterers in the coherent component affect the shape of the estimated power spectrum differently than the diffuse scatterers. Periodic scatterers cause peaks in the estimated power spectrum that degrade the fit between the estimated power spectrum and the parametric model based on diffuse scattering. The high-amplitude echo content from a specular scatterer produces a spectral estimate that is dominated by the spectral content of specular echo. Because QUS methods based on diffuse scattering involve parametric modeling of the backscattered power spectral shape, the periodic scatterers and specular scatterers also affect estimated QUS parameters. In particular, coherent scatterers can introduce bias and increase variance in the estimated QUS parameters based on diffuse scattering.

The introduction of a bias and increasing variance in the estimated QUS parameters caused by scatterers in the coherent component is undesirable when using QUS parameters based on diffuse scattering for disease detection and diagnosis by creating a tumor classification system [12]. Note that the coherent component scatterers have been shown to have diagnostic value; however, they must be treated as an aberration when estimating QUS parameters based on diffuse scatterers [13]. The goal of this present work is to develop a strategy to mitigate the effects of coherent signal components on diffuse scattering estimates, i.e., ESD. The strategy was validated using simulated and experimental backscattered signals.

## II. Methods

### A. Power Spectral Estimation

Power spectral estimates for discretely sampled ultrasonic backscattered signals can be calculated from a data block with dimensions given by axial and lateral gate lengths, corresponding to a specific location in the sample. The normalized backscattered signal power spectrum for a data block is defined as [2], [3]

$$\widehat{S}(f)=\frac{1}{L}\frac{\Re^2}{4}\sum_{l=1}^{L}\frac{S_l(f)}{S_{\text{ref}}(f)}A(f), \tag{1}$$

where $S_l(f)$ is the periodogram of the $l$th scan line segment, $S_{\text{ref}}(f)$ is the periodogram of the backscattered signal from a planar reference reflector with reflection coefficient $\Re$, $A(f)$ is a function that compensates for attenuation, and $L$ is the number of scan line segments included in the data block. To capture spatial changes in the tissue properties, data block sizes are made as small as possible (but still large enough to obtain accurate estimates) and many data blocks may be placed within a tissue region of interest (e.g., the interior of a tumor), creating a collection of data blocks for which power spectral estimates are made separately. These data blocks correspond spatially to pixels that can be color coded to a specific QUS estimate value and combined to make a map or image of the QUS parameter.

### B. ESD Parameter Estimation

The estimated power spectrum can be parameterized to provide additional information about tissue microstructure. One such parameter that has been used to characterize tissue microstructure is the ESD [2], [7]. The ESD is useful because it can provide a geometrical interpretation of the characteristic underlying tissue microstructure responsible for scattering of ultrasound. The ESD parameter can be estimated by minimizing the function [2]

$$\begin{aligned} \text{ESD} &= 2 \underset{a}{\operatorname{argmin}} \left( \int_{f_{\min}}^{f_{\max}} (X(f,a) - \overline{X})^2 \, \mathrm{d}f \right) \\ X(f,a) &= 10 \log \left( \frac{\widehat{S}(f)}{f^4 F(f,a)} \right), \end{aligned} \tag{2}$$

where $\overline{X}$ is the mean value of $X(f, a)$ within the frequency analysis bandwidth, $F(f, a)$ is the form factor, and $a$ is the effective scatterer radius parameter for the scattering model. The form factor is a model of the scatterer size, shape, and acoustic impedance structure. In this work, a spherical Gaussian form factor was used [2]. After the ESD parameter has been estimated, the effective acoustic concentration (EAC), defined as the product of the scatterer number concentration and the relative impedance difference squared, can be estimated by comparing the measured power spectrum to a theoretical power spectrum as described in [2], [11], and [12].

### C. Data Block Sorting

To reduce the effects of the coherent component on spectral-based QUS estimates, data blocks that included echoes from the coherent component were identified and sorted into a coherent scattering group and data blocks that only contained echoes from the diffuse component were sorted into a diffuse scattering group. The data blocks in the diffuse scattering group were then used to characterize the diffuse scatterers in the medium through QUS procedures.

To sort the data blocks into diffuse or coherent categories, a parameter must first be identified that accurately tracks whether the signal from the data block is dominated by diffuse or coherent scattering. For example, if the parameter increases in value when echoes from the coherent signal component are present, it may be possible to sort the data blocks into diffuse and coherent scattering groups by selecting a parameter threshold value. Several parameters were explored for the purpose of detecting the coherent signal component in individual data blocks. These parameters were based on two techniques: 1) the calculation of the generalized spectrum or 2) the analysis of envelope statistics.

**1) Generalized Spectrum—**The first set of parameters utilized the generalized spectrum (GS) to detect and quantify the observed spectral shape changes caused by echoes from the coherent component. Previous work has demonstrated that the GS is useful for ultrasonic tissue characterization. For example, the GS was found to be effective at estimating the

mean-scatterer spacing parameter, which is a parameter that quantifies long-range order in the coherent component [13]. In addition, GS-based breast tissue classifiers were observed to achieve superior performance in discrimination between benign and malignant breast masses compared with conventional textural analysis [13], [14].

The GS for a signal $y(t)$ is defined over the bifrequency plane and given by [13]

$$G(f_1, f_2)=E[Y(f_1)Y^*(f_2)], \tag{3}$$

where $E[\bullet]$ represents the statistical expectation operator, $Y$ is the Fourier transform of $y$, and the * superscript indicates a complex conjugate. From this equation, the GS is an expanded spectral autocorrelation function that is formed by taking the outer product of the Fourier transform of a signal with itself.

In this study, a spatial averaging method was used such that the GS was an average of estimates for each scan line in a data block. When an echo from the coherent component is present in the backscattered signal, spatial averaging produces an arbitrary phase change in the segments to be averaged, decreasing the rate at which the averaging process converges to the true GS. This effect can be reduced by using a synchronized average for the GS given by [14]

$$\widehat{G}(f_1, f_2)=\frac{1}{N}\sum_{i=1}^{N} Y_i(f_1)\exp(j2\pi f_1\tau_i)\times Y_i^*(f_2)\exp(-j2\pi f_2\tau_i), \tag{4}$$

where $N$ is the total number of segments used in the estimation process, $Y_i(f)$ is the Fourier transform of the $i$th scan line, and $\tau_i$ is the synchronization constant for the $i$th segment. When only diffuse scattering is present, the synchronization constant has no effect on the averaging process. Methods for estimating the synchronization constant are discussed in [14]. In this study, the synchronization constant was estimated by measuring the time between the start of the segment and the time when the maximum amplitude value in the signal occurred.

After estimating the GS using the described methods, computing the collapsed average (CA) over the GS provides a means to extract parameters that are related to the presence or absence of the coherent component. The CA is given by [15]

$$\widehat{C}(f')=\frac{1}{M(f')}\left|\sum_{f_2-f_1=f'}\widehat{G}(f_1, f_2)\right|, \tag{5}$$

where $f$ is a frequency difference associated with the off-diagonal components of the bifrequency plane and $M(f')$ is the total number of discrete GS points associated with the off-diagonal component $f_2 - f_1 = f'$. When no normalization is used in estimating the GS, the CA is an estimate of the autocorrelation function for the magnitude of the signal Fourier transform. The CA is normalized by the maximum value and displayed on a logarithmic scale for linear regression analysis. Examples of GS magnitudes and associated CAs for three types of scattering, i.e., diffuse, diffuse with periodically spaced, and diffuse with specular, are included in Fig. 1.

Three parameters estimated from the CA curve are correlated with the presence of specular echoes, including the total area under the CA curve, the slope of the best-fit line to the CA, and the $y$-intercept of the best-fit line to the CA [15]. The intercept and area parameters

increase in value when a specular scatterer is present, and the slope parameter decreases in value when a specular scatterer is present.

**2) Envelope Statistics—**The second set of parameters used statistical analysis of the backscattered signal envelope. Diffuse scatterers with sufficient concentrations create a Rayleigh-distributed signal envelope, which means that deviations from the Rayleigh distribution of the signal envelope can be used to detect the presence of echoes in the coherent component. For the Rayleigh distribution, the SNR parameter is defined as [16]

$$\mathrm{SNR}=\frac{\mu}{\sigma}, \tag{6}$$

where $\mu$ is the envelope mean and $\sigma$ is the envelope standard deviation. If the envelope is Rayleigh distributed, the SNR will have a value equal to $\sqrt{\pi/(4-\pi)}$ [16]. Several factors can cause the envelope to be non-Rayleigh-distributed, including periodically spaced scatterers, specular scatterers, areas of scattering with low concentrations of diffuse scatterers, and regions with multiple populations of different kinds of scatterers. It should also be noted that the Rayleigh SNR parameter is computationally inexpensive compared with the GS parameters.

To form a test parameter for diffuse scattering, let $\hat{\alpha}$ be defined in the following manner

$$\widehat{\alpha}=\left|\mathrm{SNR}-\sqrt{\frac{\pi}{4-\pi}}\right|. \tag{7}$$

By calculating the SNR and the $\hat{\alpha}$ parameter for each data block, it is possible to sort data blocks into groups dominated by diffuse scattering (with many scatterers per resolution cell) and groups dominated by coherent scattering. The main disadvantage of this parameter is that it is not possible to determine what types of non-diffuse scatterers are contained in the data block (e.g., periodic, specular, or low concentrations of diffuse scatterers).

### D. Technique Assessment Metrics

To quantify the ability of the techniques to improve performance of the estimation of QUS parameters, three metrics were used. The first metric was QUS estimate absolute error, which quantifies the accuracy of the estimation technique. As the effects of the coherent scatterers are reduced, it is hypothesized that QUS absolute error would be reduced. Calculating estimate absolute error is trivial in the case in which the actual QUS is known (e.g., simulations). However, in the case where actual QUS estimates are unknown (e.g., real tissues), a different metric is needed. The second metric was a clustering distance parameter defined using ESD and EAC estimates and used instead of absolute error for the tissue samples. As absolute error decreases, ESD and EAC mean values among the samples should start to cluster together. A tighter clustering should also result in improved classification performance of the parameters. The clustering distance parameter quantifies this clustering, and is defined as

$$d=\frac{1}{N}\sum_{i=1}^{N}\sqrt{(x_i-\bar{x})^2+(y_i-\bar{y})^2}, \tag{8}$$

where $x_i$ represents the mean ESD value of the $i$th tissue sample, $\bar{x}$ represents the mean across all tissue samples of the ESD mean values, $y_i$ represents the mean EAC value of the $i$th tissue sample, $\bar{y}$ represents the mean across all tissue samples of the EAC mean values, and $N$ represents the total number of tissue samples in the clustering distance analysis. The

third metric consisted of estimating the ESD and EAC relative standard deviations (RSD) for individual tissue samples. By mitigating the effects of the coherent scatterers on the estimation of ESD and EAC, it was hypothesized that ESD RSD and EAC RSD for individual tissue samples would be reduced.

## III. Simulations and Experiments

The proposed methods for reducing the effects of the coherent component on spectral-based QUS characterization of diffuse scatterers were tested using simulated and experimental ultrasound backscattered data. Simulated backscattered signals were specifically designed to include echoes from both the diffuse and coherent signal components. Experimental backscattered signals were specifically selected for analysis because of the presence of echoes from both diffuse and coherent signal components.

### A. Simulations

A simulated backscatter phantom was generated in Matlab (The MathWorks Inc., Natick, MA) with diffuse scatterers (10 scatterers/resolution cell) and specular scatterers (1 to 3 scatterer/$cm^3$) using a spherical Gaussian scattering model. Multiple scan lines were constructed by translating the simulated transducer laterally across the length of the phantom. A total of 25 simulated backscatter slices were collected. Diffuse scatterers were simulated using a size of 50 μm and specular scatterers simulated using a size of 100 μm (size given as the effective diameter, assuming a spherical Gaussian spatial autocorrelation function). The specular scatterers had scattering signal amplitude between 2 and 5 times that of the diffuse scatterers. The source impulse response was modeled as a modulated Rayleigh pulse with a center frequency of 10 MHz and −6-dB pulse/echo bandwidth of 5 MHz.

### B. Rat Fibroadenomas

Ultrasonic backscattered data from rats that had spontaneously developed mammary tumors (fibroadenomas) were analyzed. Tumor diameters ranged in size from 1 to 6 cm. In an experiment, the animal was mounted in a custom-designed holder that allowed direct access to the tumor site. The animal was euthanized and placed in a tank of degassed room temperature water for scanning. A focused transducer with a nominal center frequency of 7.5 MHz (f/4) and a −6-dB frequency bandwidth of 6 MHz was used to scan the tumors. The transducer was moved using a computer-controlled micro-positioning system while the sample was held stationary. Five 2-D B-mode slices separated by 1 mm were acquired for each animal. Scan lines were separated by 150 μm. After the scans, the tumors were excised, fixed in formalin, trimmed for histology, and sent for pathology. For this study, all of the analyzed tumors were fibroadenomas and only tumor slices with at least one identified specular scatterer on the interior region of the tumor were analyzed. Reference scans were acquired for the transducer from a poly(methyl methacrylate) (PMMA) reflector, using the same equipment settings as were used for the tumor imaging. The attenuation assumed for the tumors was 0.9 dB/cm/MHz [7]. A total of 10 tumor slices were analyzed for this study, representing 6 tumor samples.

### C. Beef Livers

Experimental backscattered signals were analyzed from 6 fresh beef liver samples scanned at a temperature of 37°C. Multiple specular scatterers were visible in the beef livers, possibly because of the presence of blood vessels. The samples were completely submerged in 0.9% saline solution made from degassed water and a 20-MHz single-element transducer (f/3) with −10-dB bandwidth of 18 MHz was used for scanning. The transducer was moved using a computer-controlled micro-positioning system while the sample was held stationary. A total of 30 adjacently spaced scan lines with a lateral step size of 200 μm (approximately

one full beam width) were collected for each sample. Sound speed and attenuation were estimated using an insertion loss method. Reference scans were acquired for the transducer from a PMMA reflector, using the same equipment settings as were used for the beef liver imaging.

## IV. Results

Examples of B-mode images for simulated and experimental backscatter slices are shown in Figs. 2(a)–2(c). Numerous coherent scatterers are evident in the B-mode image slices as bright spots. After selecting a larger analysis region and segmenting the image into overlapping data blocks (75% data block overlap was used), the QUS parameters were estimated for each data block and ESD parametric images were created. The ESD parametric images overlaid on the B-mode images of the examined backscattered slices are shown in Figs. 2(d)–2(f). From the ESD parametric images, it can be observed that the coherent scatterers had a significant effect on the estimation of the ESD parameter. Areas that included and were near coherent scatterers had significantly increased or decreased ESD estimates that reflected the sizes of the coherent scatterers and not the surrounding diffuse scatterers.

The data block sorting method was applied to the data in Fig. 2 to reduce the effects of the coherent component. Parametric images were then formed using only the data blocks in the diffuse scattering group. The resulting modified ESD parametric images are shown in Figs. 2(g)–2(i). From these parametric images, it can be observed that the data block sorting method significantly reduced the effects of the coherent scatterers on the ESD parametric images. For the fibroadenoma example, although significant variation of the ESD estimates is still visible after sorting data blocks, it is now apparent that this variation is not due to the visible non-diffuse echoes. For the beef liver example, although only 3 data blocks were sorted into the diffuse scattering group, the variation among these three ESD estimates is much less than the variation when considering all of the data blocks.

### A. Simulation Results

For the simulation data, Fig. 3 shows an example of the error curves versus the parameter threshold value using the GS intercept for one tissue sample. The ESD absolute error and ESD RSD decreased as the threshold value decreased, leading to more accurate estimates. The decreasing threshold value resulted in more sensitivity to coherent signal contributions and also resulted in increasingly more data blocks being sorted out of the diffuse scattering group (see Fig. 4). Therefore, fewer data blocks would be available to characterize the sample or to form an image. The ESD absolute error actually increased when the threshold was −8-dB or lower, probably because fewer than 15% of the data blocks were sorted into the diffuse scattering group.

As the parameter threshold value is changed, the number of data blocks sorted into the diffuse scattering group can decrease. If the threshold value is chosen to be too large, all of the data blocks can be sorted out of the diffuse scattering group. Therefore, the threshold value must be chosen so that it can detect strong coherent signals, but not be too sensitive to smaller coherent signals.

ESD absolute error curves similar to the one in Fig. 3(a) were formed for each of the 25 simulated slices. An average ESD absolute error curve was formed by averaging across the 25 slices. In addition, percentage of data blocks sorted in the diffuse scattering group curves similar to the one in Fig. 4 were formed for each of the 25 simulated slices. An average percentage of data blocks sorted into the diffuse scattering group curve was formed by averaging across the 25 slices. The average ESD absolute error curve was displayed as a

function of the average percentage of data blocks sorted into the diffuse scattering group. This process was repeated for each of the available sorting parameters, including the GS intercept, slope, area, and the Rayleigh SNR parameter. The results of the analysis are shown in Fig. 5(a). The process was repeated for the ESD RSD curves to produce average ESD RSD curves as a function of the percentage of data blocks sorted into the diffuse scattering group for each of the tested sorting parameters. The results of the analysis are shown in Fig. 5(b).

The absolute error and RSD analysis revealed that the GS intercept, GS area, and Rayleigh SNR sorting parameters reduced the ESD absolute error and ESD RSD while sorting the largest percentage of data blocks into the diffuse scattering group. An elbow in the error curves exists when roughly 50% of the data blocks have been sorted into the diffuse scattering group for each of these sorting parameters. Therefore, the threshold could be selected for these parameters by selecting the parameter value that sorted this percentage of data blocks into the diffuse scattering group. The GS slope parameter produced similar performance compared with the other parameters, except performance degraded for this parameter when fewer than 60% of data blocks were sorted into the diffuse scattering group compared with the other parameters.

### B. Rat Fibroadenoma Results

The data block sorting method was applied to the fibroadenoma samples and sorting parameter performance was compared using a method that was similar to that applied to the simulated backscattered samples. For each slice, the clustering distance parameter defined in Section III, the ESD RSD, and the EAC RSD were found as a function of the parameter threshold. The resulting curves were averaged and displayed as a function of the average percentage of data blocks sorted into the diffuse scattering group. The results are shown in Fig. 6.

From Fig. 6(a), it can be observed that in the range of 75 to 100% of data blocks sorted into the diffuse scattering group, the GS intercept and GS slope parameters produced the lowest clustering distance mean among the analyzed slices. In the range from 50 to 75% of data block sorted into the diffuse scattering group, the Rayleigh SNR and the GS area parameters produced the lowest clustering distance mean among the analyzed slices. In the range from 25 to 50% of data block sorted into the diffuse scattering group, the Rayleigh SNR parameter produced the lowest clustering distance mean among the analyzed slices. From Fig. 6(b), it can be observed that in the range from 80 to 100% of data blocks sorted into the diffuse scattering group, the Rayleigh SNR and the GS intercept produced the lowest ESD RSD. In the range from 20 to 80%, the Rayleigh SNR parameter produced the lowest ESD RSD. From Fig. 6(c), it can be observed that in the range from 90 to 100% of data blocks sorted into the diffuse scattering group, the Rayleigh SNR and the GS intercept produced the lowest EAC RSD. In the range from 20 to 90%, the Rayleigh SNR parameter produced the lowest EAC RSD. Note that the GS area parameter appears to be cut off in the middle of the graph because, for one of the samples, all data blocks had been sorted into the coherent scattering group for the associated parameter threshold value.

The results for the fibroadenoma samples indicated that the Rayleigh SNR parameter produced the greatest clustering of ESD mean and EAC mean values for the collection of fibroadenomas and the greatest average reduction in ESD RSD and EAC RSD for individual fibroadenomas. Therefore, this parameter was selected as the best sorting parameter for the fibroadenoma samples. The threshold for the Rayleigh SNR sorting parameter was selected by minimizing the clustering distance mean value. The curve recording clustering distance mean displayed as a function of the Rayleigh SNR parameter is shown in Fig. 7. From Fig. 7, the minimum clustering distance mean occurred when the parameter threshold was set to

0.5. Therefore, this value was used as the sorting parameter threshold. To demonstrate the ability of the data block sorting method to reduce the effects of the coherent signal, the ESD and EAC mean values were found for each fibroadenoma. Fibroadenomas were displayed according to their ESD and EAC mean values as shown in Fig. 8(a). The data block sorting method was applied to each fibroadenoma using the Rayleigh SNR as the sorting parameter and 0.5 as the sorting threshold and the ESD and EAC statistics were recalculated and shown in Fig. 8(b). From Fig. 8, it can be observed that the data block sorting method significantly reduced error bar lengths and caused the fibroadenomas to be clustered closer together compared with not using the data block sorting method. Therefore, the data block sorting method causes greater clustering of the ESD mean values compared with the EAC mean values. Typically, the EAC has a much greater range of values than the ESD and is therefore logarithmically compressed before recording the value. Therefore, changes in EAC mean values resulting from the data block sorting method will not have as great of an effect on EAC estimates, leading to reduced clustering of the EAC mean values.

### C. Beef Liver Results

The data block sorting method was applied to the beef liver samples and sorting parameter performance was compared using the same method applied to the fibroadenomas. For each slice, the clustering distance parameter defined in Section III, the ESD RSD, and the EAC RSD were found as a function of the parameter threshold. The resulting curves were averaged and then displayed as a function of the average percentage of data blocks sorted into the diffuse scattering group. The results are shown in Fig. 9.

From Fig. 9(a), it can be observed that in the range from 80 to 100% of data blocks sorted into the diffuse scattering group, the GS intercept and Rayleigh SNR parameters produced the lowest clustering distance means. In the range from 55 to 80% of data blocks sorted into the diffuse scattering group, the Rayleigh SNR parameter produced the lowest clustering distance mean. In the range from 35 to 55% of data blocks sorted into the diffuse scattering group, the GS intercept parameter produced the lowest clustering distance mean. From Fig. 9(b), it can be observed that in the range from 85 to 100% of data blocks sorted into the diffuse scattering group, the GS area parameter produced the lowest ESD RSD values. In the range from 55 to 85% of data blocks sorted into the diffuse scattering group, the Rayleigh SNR and the GS intercept parameters produced the lowest ESD RSD values. In the range from 20 to 55% of data blocks sorted into the diffuse scattering group, the GS area parameter produced the lowest ESD RSD values. Similar trends were observed in Fig. 9(c) for the EAC RSD.

Based on reducing the clustering distance mean, the GS intercept parameter was selected as the best sorting parameter. The threshold for the GS intercept sorting parameter was selected by minimizing the clustering distance mean. The curve recording clustering distance mean displayed as a function of the GS intercept parameter is shown in Fig. 10. From Fig. 10, it can be observed that the minimum clustering distance mean occurs when the parameter threshold was set to −3.2 dB. At this threshold value (and at the associated average percentage of data blocks sorted into the diffuse scattering group), the GS intercept parameter also produced low ESD RSD and EAC RSD values compared with the other sorting parameters.

To demonstrate the ability of the data block sorting method to reduce the effects of the coherent signal, the ESD mean and EAC mean values were found for each beef liver sample. Beef liver samples were then displayed according to their ESD and EAC mean values and shown in Fig. 11(a). Next, using the GS intercept sorting parameter, data blocks for each sample were sorted according to the −3.2-dB threshold and the ESD and EAC statistics were recalculated and shown in Fig. 11(b). From Fig. 11, it can be observed that the data block

sorting method significantly reduced error bar lengths and caused the beef liver samples to be clustered closer together compared with not using the data block sorting method. Similar to the fibroadenoma samples, it is observed from Fig. 11 that the data block sorting method causes greater clustering of the ESD mean values compared with the EAC mean values.

## V. Discussion

The main contribution of this work is a method to limit the effects of specular echoes on QUS parameter estimation for diffuse scatterers through the sorting of data blocks into diffuse and non-diffuse scattering groups. When implementing this method, selection of the sorting parameter and accompanying selection of the parameter threshold proved to be the most difficult tasks. In this study, these tasks were accomplished for distinct collections of tissue types (i.e., simulation, fibroadenoma, and beef liver). Each tissue collection was examined separately from the other tissue collections. For the simulated data, true size values for the diffuse scatterers were known *a priori*; therefore, it was possible to use absolute ESD error to select the sorting parameter and sorting threshold. For the physical tissues, true scatterer sizes were not known beforehand; therefore, the clustering distance parameter was designed using the hypothesis that as absolute error decreases, ESD and EAC mean values among the samples should start to cluster together.

For simulations, the best performing parameters in terms of reducing ESD absolute error and ESD RSD included the GS intercept, GS area, and Rayleigh SNR parameters. For the fibroadenoma tumors, the best performing parameter for reducing the clustering distance was the Rayleigh SNR parameter. For the beef liver samples, the best performing for reducing the clustering distance was the GS intercept parameter, followed closely by the Rayleigh SNR parameter. Considering the results from simulations, fibroadenoma, and beef liver samples, the Rayleigh SNR parameter was the sorting parameter that consistently produced the best results or very close to the best results.

Implementation of this method in the future will depend on several factors, including whether a tissue collection includes one or more tissue samples and what the purpose is for reducing the effects of the non-diffuse echoes. If a single tissue sample is available for analysis, then the ESD RSD and EAC RSD could be used to select a parameter threshold for the Rayleigh SNR parameter. The ESD RSD and EAC RSD do not require a collection of samples because these metrics can be applied to individual samples. For the simulations, the ESD RSD and EAC RSD typically exhibited behavior similar to that observed in Fig. 5(b), displaying a shoulder point where the metric reached a minimum value for a certain sorting parameter threshold and maintained that value when sorting more data blocks into the non-diffuse scattering group. For physical tissues, this type of behavior did not occur as frequently as it did for the simulations. If the behavior does occur, then it makes sense to pick the shoulder point as the sorting parameter threshold. If this shoulder behavior does not exist, then the ESD RSD or EAC RSD could still be minimized; however, it would be necessary to constrain the problem such that there would be a minimum percentage of data blocks sorted into the diffuse scattering group (e.g., 20%), otherwise the minimum RSD would occur when one data block remained in the diffuse scattering group. If multiple tissue samples are available and the ESD and EAC mean values are being used as features in a tissue classification system, then the clustering distance parameter can be used for parameter threshold selection. Based on the fibroadenoma and beef liver tissue, the Rayleigh SNR parameter should be used to improve clustering.

For the simulations, all parameters (except the GS slope) performed similarly in terms of reducing ESD absolute error and ESD RSD. As observed in Fig. 5, the GS slope parameter did not have a shoulder point similar to the other examined parameters. This behavior

indicates that the GS slope had decreased sensitivity to specular echoes with amplitudes close to that of the diffuse echoes compared with the other parameters.

For the fibroadenoma slices, the behavior of the clustering distance in Fig. 6(a) had irregular shape for both the ESD RSD and EAC RSD. The GS intercept and GS slope parameters performed best in the range of 75 to 100% of data blocks sorted into the diffuse scattering group, the Rayleigh SNR and GS area parameters performed best in the range from 50 to 75% of data blocks sorted into the diffuse scattering group, and the Rayleigh SNR performed best in the range from 25 to 50% of data blocks sorted into the diffuse scattering group. In contrast, the Rayleigh SNR parameter performed best in terms of reducing ESD RSD and EAC RSD in the range from 20 to 90% of data blocks sorted into the diffuse scattering group. Reducing ESD or EAC RSD is a less difficult task compared with reducing the clustering distance parameter, causing the cluster distance analysis in Fig. 6(a) to appear to be more complex than the ESD RSD and EAC RSD analysis in Figs. 6(b) and 6(c), respectively.

For the beef liver slices, the clustering distance curves, ESD RSD, and EAC RSD all appeared to have irregular shape. For the ESD RSD and EAC RSD, all of the parameters performed comparably and none offered significant reductions in ESD RSD or EAC RSD in the range of 50 to 100% of data blocks sorted into the diffuse scattering group. The beef liver samples tended to contain very few specular echoes (zero, one, or two) or many specular echoes such that it was difficult to place data blocks that did not include non-diffuse echoes. It is for this reason that all of the plots in Fig. 6 do not appear smooth.

When coherent scatterers existed in low concentrations and were sparsely located, the data block sorting method was sufficient to limit their effects on QUS. However, in the case that coherent scatterers existed in higher concentrations and were more densely located, the data block sorting method was not very successful because it was only possible to select a small number of data blocks that only included diffuse echoes. An example of this case is Fig. 2(i), in which only three data blocks were sorted into the diffuse scattering group.

For simulations, fibroadenoma samples, and beef liver samples, the parameter threshold was selected such that roughly 50% of the data blocks were sorted into the diffuse scattering group. The number of data blocks sorted into the diffuse scattering group varied greatly depending on the number of specular echoes detected in the region. In addition, because data blocks were overlapped by 75%, sorting 50% of the data blocks into the diffuse scattering group did not necessarily cause most of the examined region to be excluded from the analysis of diffuse scatterers.

## VI. Conclusion

When using QUS parameters designed to characterize diffuse scatterers, it is important to pursue actions that reduce or eliminate the effects of coherent scatterers. The method proposed in this work for accomplishing this task focused on identifying backscattered signal sections that included coherent echoes and then removing these sections of the backscattered signal from the QUS analysis of the medium. Individual data blocks that included coherent echoes were identified using a sorting parameter and removed from the analysis of diffuse scatterers.

The proposed method was studied using simulated and experimental ultrasonic backscattered signals. Results indicated that the proposed strategies successfully reduced or eliminated the effects of the coherent scatterers on the QUS analysis of diffuse scatterers. Across the different tissue collections, the Rayleigh SNR parameter provided the best performance in terms of reducing ESD absolute error (for simulation) and reducing the

clustering distance parameter (for physical tissues). The results indicated that it was possible to sort data blocks in such a way as to promote clustering of ESD and EAC mean values. The improvement in the clustering distance parameter suggests that the method would improve the ESD and EAC as features for tissue classification by reducing the effects of non-diffuse echoes on QUS estimation.

## Acknowledgments

The authors thank Dr. R. J. Miller and J. P. Blue, Jr. for assistance in obtaining the tissue samples.

This research was supported by National Institutes of Health grant R01CA111289.

## References

1. Lizzi FL, Greenbaum M, Feleppa EJ, Elbaum M, Coleman DJ. Theoretical framework for spectrum analysis in ultrasonic tissue characterization. J. Acoust. Soc. Am. 1983 Apr.vol. 73:1366–1373. [PubMed: 6853848]
2. Insana MF, Wagner RF, Brown DG, Hall TJ. Describing small-scale structure in random media using pulse-echo ultrasound. J. Acoust. Soc. Am. 1990 Jan; vol. 87(no.1):179–192. [PubMed: 2299033]
3. Insana MF, Hall TJ. Parametric ultrasound imaging from backscatter coefficient measurements: Image formation and interpretation. Ultrason. Imaging. 1990 Oct.vol. 12:245–267. [PubMed: 1701584]
4. Feleppa EJ, Lizzi FL, Coleman DJ, Yaremko MM. Diagnostic spectrum analysis in ophthalmology: A physical perspective. Ultrasound Med. Biol. 1986 Aug; vol. 12(no.8):623–631. [PubMed: 3532476]
5. Feleppa EJ, Kalisz A, Sokil-Melgar JB, Lizzi FL, Liu T, Rosado AL, Shao MC, Fair WR, Wang Y, Cookson MS, Reuter VE, Heston WDW. Typing of prostate tissue by ultrasonic spectrum analysis. IEEE Trans. Ultrason. Ferroelectr. Freq. Control. 1996 Jul; vol. 43(no.4):609–619.
6. Lizzi FL, King DL, Rorke MC, Hui J, Ostromogilsky M, Yaremko MM, Feleppa EJ, Wai P. Comparison of theoretical scattering results and ultrasonic data from clinical liver examinations. Ultrasound Med. Biol. 1988; vol. 14(no.5):377–385. [PubMed: 3051612]
7. Oelze ML, O'Brien WD Jr, Blue JP, Zachary JF. Differentiation and characterization of rat mammary fibroadenomas and 4T1 mouse carcinomas using quantitative ultrasound imaging. IEEE Trans. Med. Imaging. 2004 Jun; vol. 23(no.6):764–771. [PubMed: 15191150]
8. Insana MF, Wagner RF, Garra BS, Brown DG, Shawker TH. Analysis of ultrasound image texture via generalized Rician statistics. Opt. Eng. 1986 Jun; vol. 25(no.6):743–748.
9. Abeyratne UR, Petropulu AP, Reid JM. On modeling the tissue response from ultrasonic B-scan images. IEEE Trans. Med. Imaging. 1996 Aug; vol. 15(no.4):479–490. [PubMed: 18215929]
10. Georgiou G, Cohen FS. Tissue characterization using the continuous wavelet transform. Part I: Decomposition method. IEEE Trans. Ultrason. Ferroelectr. Freq. Control. 2001 Mar; vol. 48(no. 2):355–363. [PubMed: 11370349]
11. Oelze ML, O'Brien WD Jr. Improved scatterer property estimates from ultrasound backscatter for small gate lengths using a gate-edge correction factor. J. Acoust. Soc. Am. 2004 Nov.vol. 116:3212–3223. [PubMed: 15603167]
12. Oelze ML, O'Brien WD Jr, Blue JP, Zachary JF. Differentiation and characterization of rat mammary fibroadenomas and 4T1 mouse carcinomas using quantitative ultrasound imaging. IEEE Trans. Med. Imaging. 2004 Jun.vol. 23:764–771. [PubMed: 15191150]
13. Varghese T, Donohue KD. Mean-scatterer spacing estimates with spectral correlation. J. Acoust. Soc. Am. 1994; vol. 96(no.6):3504–3515. [PubMed: 7814765]
14. Donohue KD, Forsberg F, Piccoli CV, Goldberg BB. Analysis and classification of tissue with scatterer structure templates. IEEE Trans. Ultrason. Ferroelectr. Freq. Control. 1999; vol. 46(no.2): 300–310. [PubMed: 18238426]

15. Donohue KD, Huang L, Burks T, Forsberg F, Piccoli CW. Tissue classification with generalized spectrum parameters. Ultrasound Med. Biol. 2001; vol. 27(no.11):1505–1514. [PubMed: 11750750]

16. Shankar PM, Reid JM, Ortega H, Piccoli CW, Goldberg BB. Use of non-Rayleigh statistics for the identification of tumors in ultrasonic B-scans of the breast. IEEE Trans. Med. Imaging. 1993 Dec; vol. 12(no.4):687–692. [PubMed: 18218463]

## Biographies

**Adam C. Luchies** was born in Ann Arbor, MI, in 1987. He graduated from John Brown University, Siloam Springs, AR, in 2009 with a B.S. degree in engineering. He started his graduate studies in the Bioacoustics Research Laboratory at the University of Illinois at Urbana-Champaign in 2009. He earned his M.S. degree in electrical and computer engineering in 2011 and is now pursuing a Ph.D. degree in the same field. His research interests include ultrasound imaging, ultrasonic tissue characterization, quantitative ultrasound, and spectral estimation.

**Goutam Ghoshal** was born in Kolkata, India, in 1978. He earned his B.E. degree in mechanical engineering in 2000 from University of Pune, Pune, India, and his M.S. and Ph.D. degrees in engineering mechanics from the University of Nebraska–Lincoln in 2003 and 2008, respectively. Dr. Ghoshal is currently a Postdoctoral Research Associate at the University of Illinois at Urbana- Champaign, where he is conducting research in medical ultrasound. His research interests include ultrasonic wave propagation in heterogeneous media, quantitative ultrasound, ultrasound tissue characterization, ultrasound imaging, and computation methods for ultrasonic wave propagation in random media.

**William D. O'Brien, Jr.** is the Donald Biggar Willet Professor of Engineering, Department of Electrical and Computer Engineering, University of Illinois at Urbana-Champaign. From 1971 to 1975, he worked with the Bureau of Radiological Health (currently CDRH) of the U.S. Food and Drug Administration. Since 1975, he has been at the University of Illinois, where he is the Donald Biggar Willet Professor of Engineering. He also is Professor of Electrical and Computer Engineering and of Bioengineering, College of Engineering; Professor of Bioengineering, College of Medicine; Professor of Nutritional Sciences, College of Agricultural, Consumer and Environmental Sciences; and Research Professor in

the Beckman Institute for Advanced Science and Technology. He is the Director of the Bioacoustics Research Laboratory. His research interests involve the many areas of acoustic– and ultrasound–tissue interaction, including biological effects and quantitative acoustic imaging, for which he has published 368 papers, and has recently received an NIH MERIT (R37) award. Dr. O'Brien's research deals with the mechanisms by which acoustic energy interacts with biological and non-biological materials (physical acoustics), and applications of quantitative acoustic imaging in biology, agriculture, material science, and medicine. The physical acoustics research activities focus on the fundamental understanding of how ultrasound interacts with biological materials, and specifically the role of heat and cavitation, and their relationship to the assessment of risk for the safe application of clinical ultrasound. The applications of quantitative acoustic imaging research activities focus on the development of novel techniques to improve the quality of life, including solid tumor diagnosis and *in vivo* ultrasonic microprobe sensor for tumor diagnosis.

Dr. O'Brien is a Fellow of the Institute of Electrical and Electronics Engineers, the Acoustical Society of America, and the American Institute of Ultrasound in Medicine, and is a Founding Fellow of the American Institute of Medical and Biological Engineering. He was recipient of the IEEE Centennial Medal (1984), the AIUM Presidential Recognition Awards (1985 and 1992), the AIUM/WFUMB Pioneer Award (1988), the IEEE Outstanding Student Branch Counselor Award for Region 4 (1989), the AIUM Joseph H. Holmes Basic Science Pioneer Award (1993), and the IEEE Ultrasonics, Ferroelectrics, and Frequency Control Society Distinguished Lecturer (1997–1998). He received the IEEE Ultrasonics, Ferroelectrics, and Frequency Control Society's Achievement Award for 1998 and Distinguished Service Award for 2003, and the IEEE Millennium Medal in 2000. He also received the Rayleigh Award for 2008 from the IEEE Ultrasonics, Ferroelectrics, and Frequency Control Society. He has served as Co-Chair of the 1981, 2001, and 2003 IEEE Ultrasonic Symposia, and General Chair of the 1988 IEEE Ultrasonics Symposium. He has served as President (1982–1983) of the IEEE Sonics and Ultrasonics Group (currently the IEEE Ultrasonics, Ferroelectrics, and Frequency Control Society), Editor-in-Chief (1984–2001) of the *IEEE Transactions on Ultrasonics, Ferroelectrics, and Frequency Control*, President (1988–1991) of the American Institute of Ultrasound in Medicine, and Treasurer (1991–1994) of the World Federation for Ultrasound in Medicine and Biology, and has served on the Board of Directors (1988–1993) of the American Registry of Diagnostic Medical Sonographers.

**Michael Oelze** was born in Hamilton, New Zealand, in 1971. He earned his B.S. degree in physics and mathematics in 1994 from Harding University, Searcy, AR; his M.S. degree in physics in 1996 from the University of Louisiana at Lafayette, Lafayette, LA; and his Ph.D. degree in physics in 2000 from the University of Mississippi, Oxford, MS. Dr. Oelze was a postdoctoral fellow at the University of Illinois at Urbana-Champaign from 2000 to 2004, conducting research in ultrasound. Currently, Dr. Oelze is an assistant professor in the Department of Electrical and Computer Engineering at the University of Illinois at Urbana-Champaign. His research interests include the acoustic interaction with soil, ultrasound tissue characterization, quantitative ultrasound, ultrasound bioeffects, ultrasound tomography techniques, therapeutic ultrasound, and application of coded excitation to

ultrasound imaging. Dr. Oelze is a member of the ASA, a senior member of IEEE and the IEEE UFFC Society, and a fellow of the AIUM.

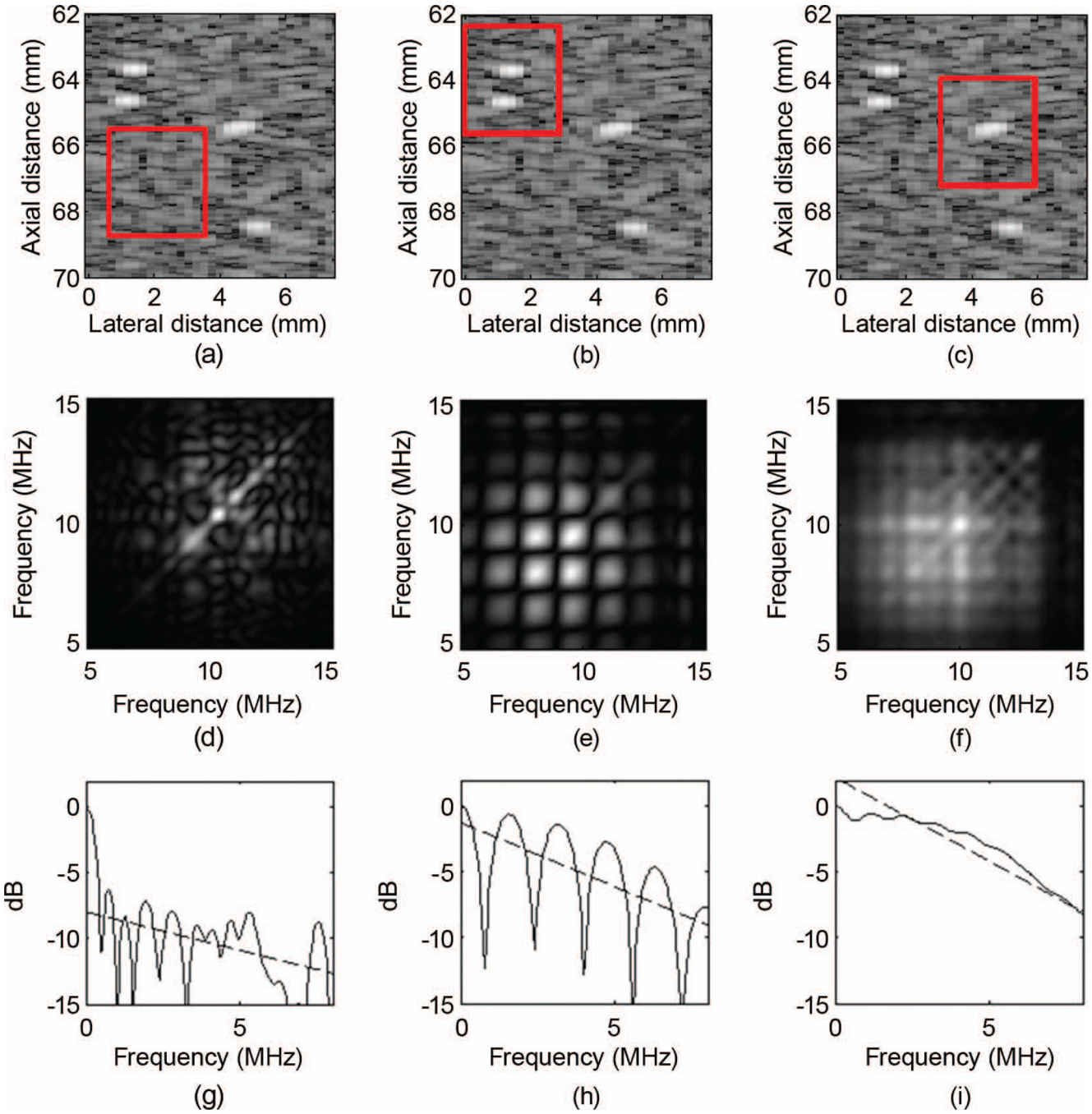


**Fig. 1.**

Examples of data blocks (outlined using boxes) with (a) diffuse, (b) periodic with diffuse, and (c) specular with diffuse scatterers. Associated (d)–(f) generalized spectra, and (g)–(i) collapsed averages. The slopes of the linear fit to the collapsed averages in (g)–(i) are −0.59, −0.98, and −1.4, respectively. The intercepts of the linear fit to the collapsed averages in (g)–(i) are −7.9, −1.2, and 0.55, respectively.

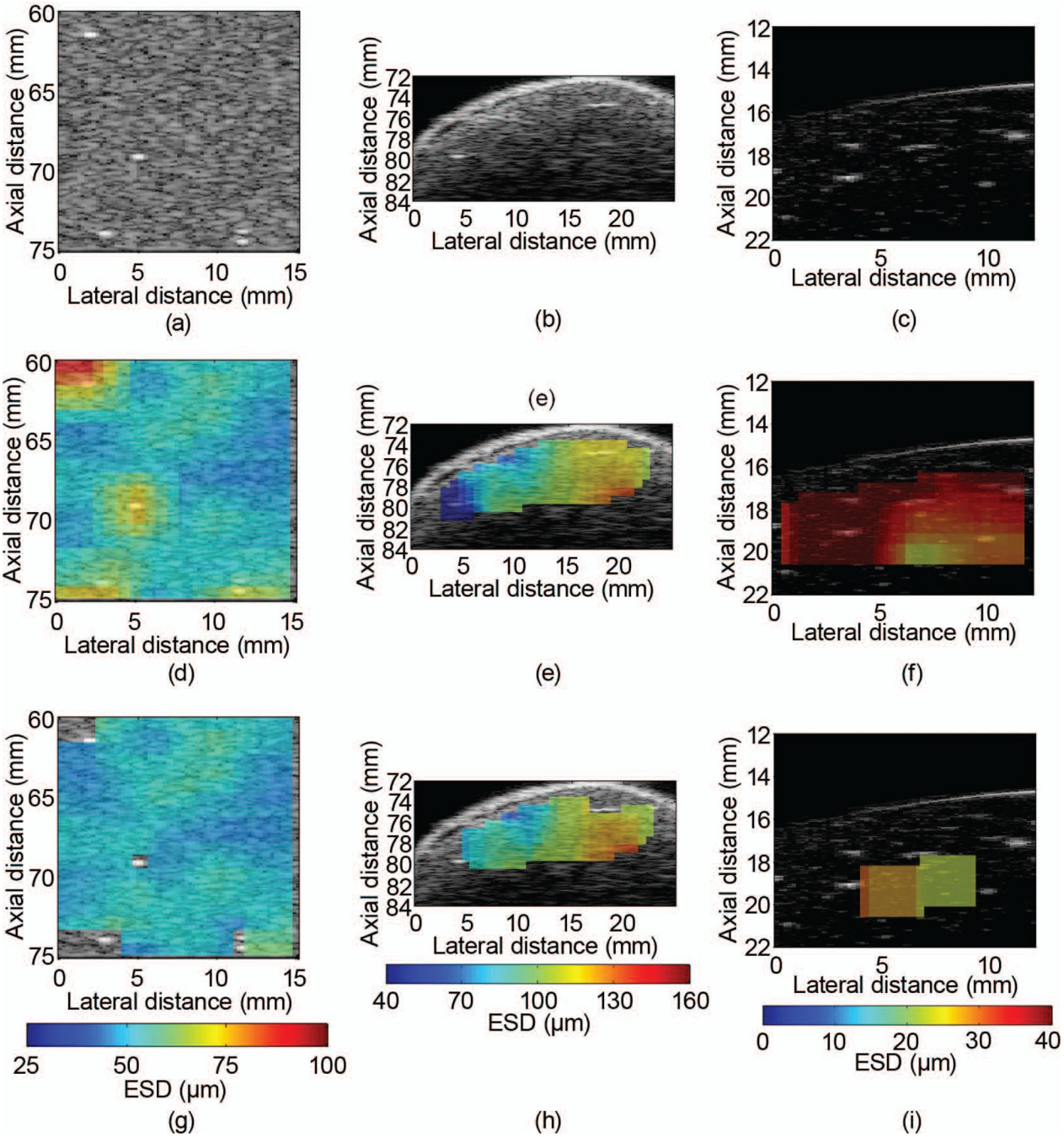


**Fig. 2.**

Examples of (a)–(c) B-mode images, (d)–(f) effective scatterer diameter (ESD) parametric images, and (g)–(i) ESD parametric images when using the data block sorting method for simulation (left), fibroadenoma (middle column), and beef liver (right).

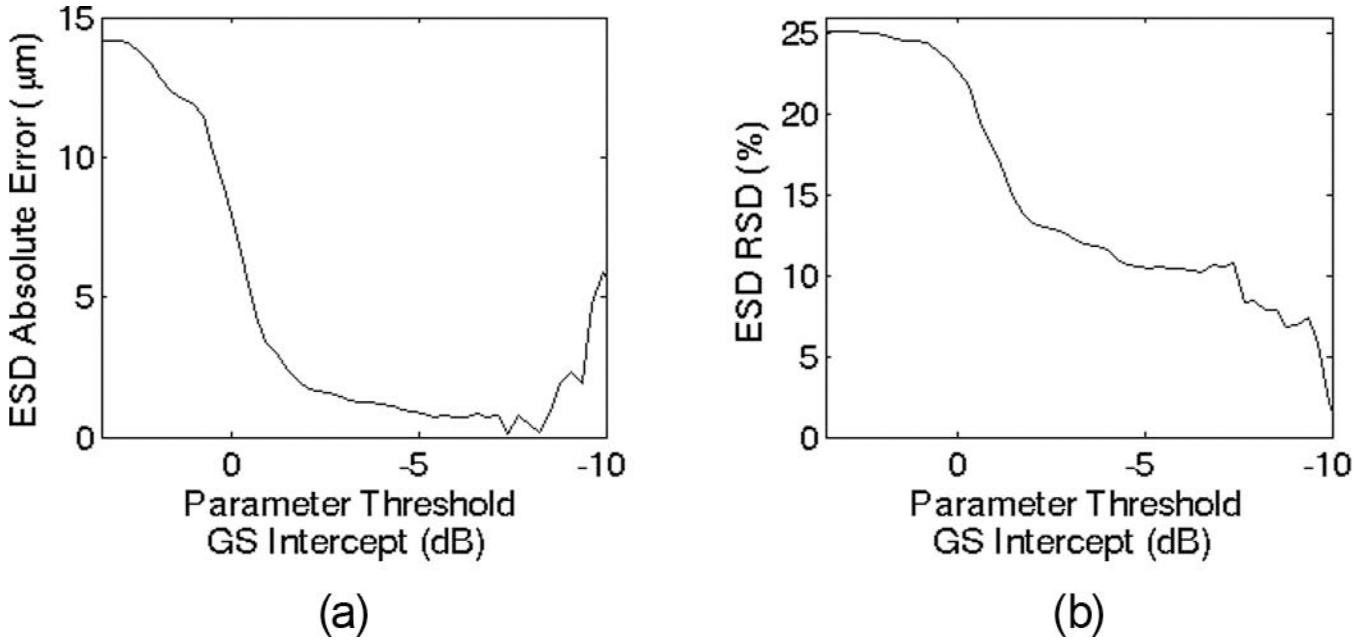


**Fig. 3.**

Effective scatterer diameter (ESD) estimate (a) absolute error and (b) relative standard deviation as a function of the sorting parameter threshold value for one simulated backscatter slice. The generalized spectrum (GS) intercept parameter is being used as the sorting parameter in this example.

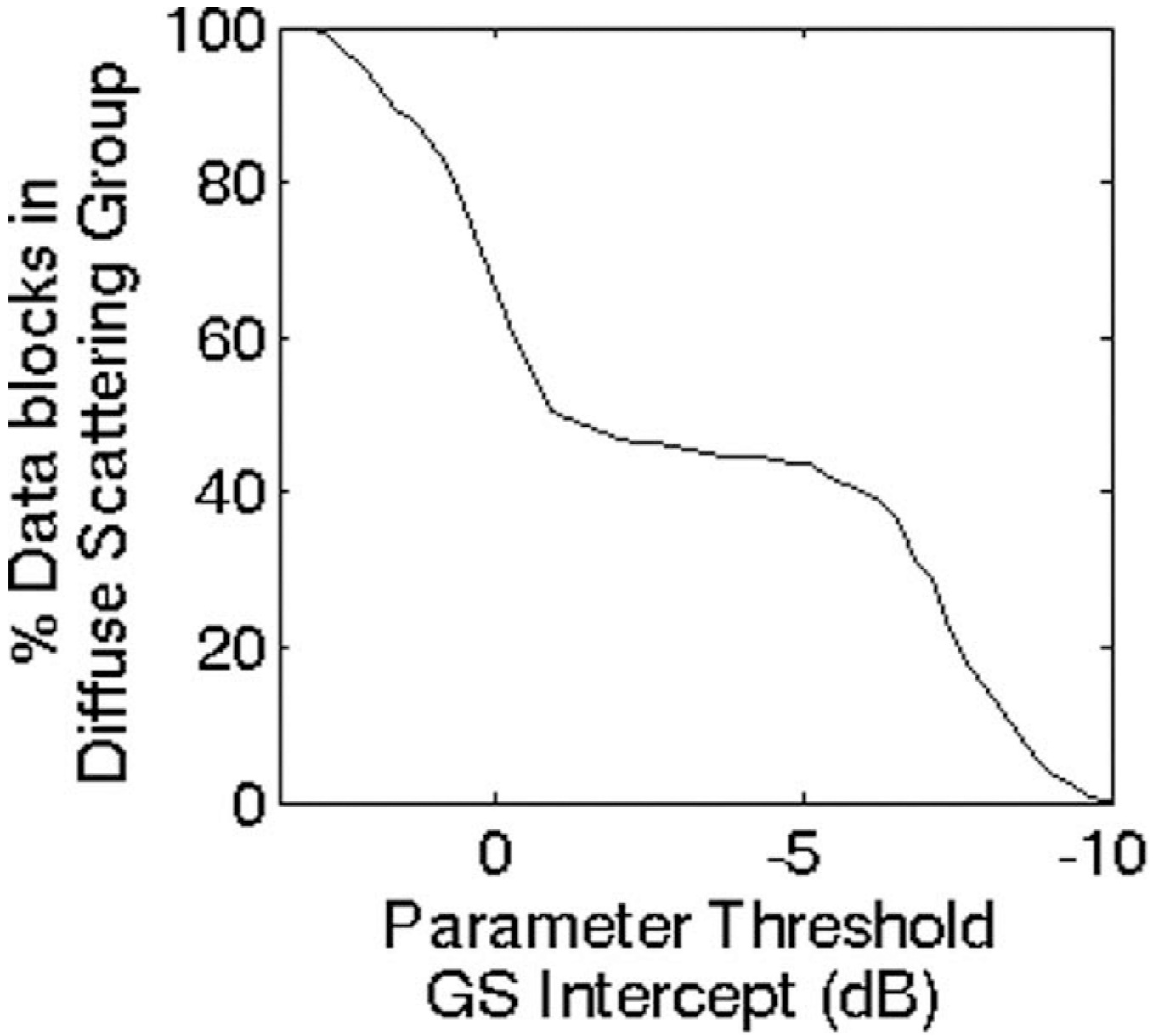


**Fig. 4.**

Percentage of data blocks sorted into the diffuse scattering group as a function of the sorting parameter threshold value for one simulated backscatter slice. The generalized spectrum (GS) intercept parameter is being used as the sorting parameter in this example.

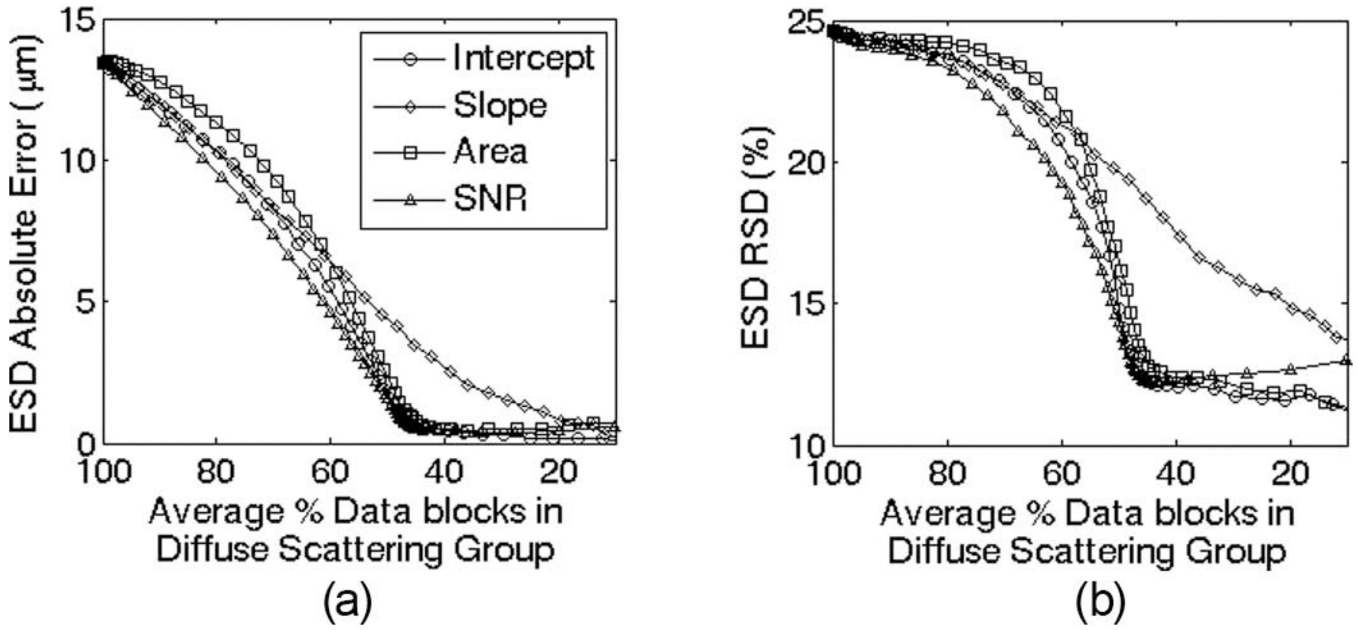


**Fig. 5.**

Effective scatterer diameter (ESD) estimate (a) absolute error and (b) relative standard deviation (RSD) curves for the data blocks in the diffuse scattering group averaged over the analyzed simulated slices and displayed as a function of the average percentage of data blocks sorted into the diffuse scattering group.

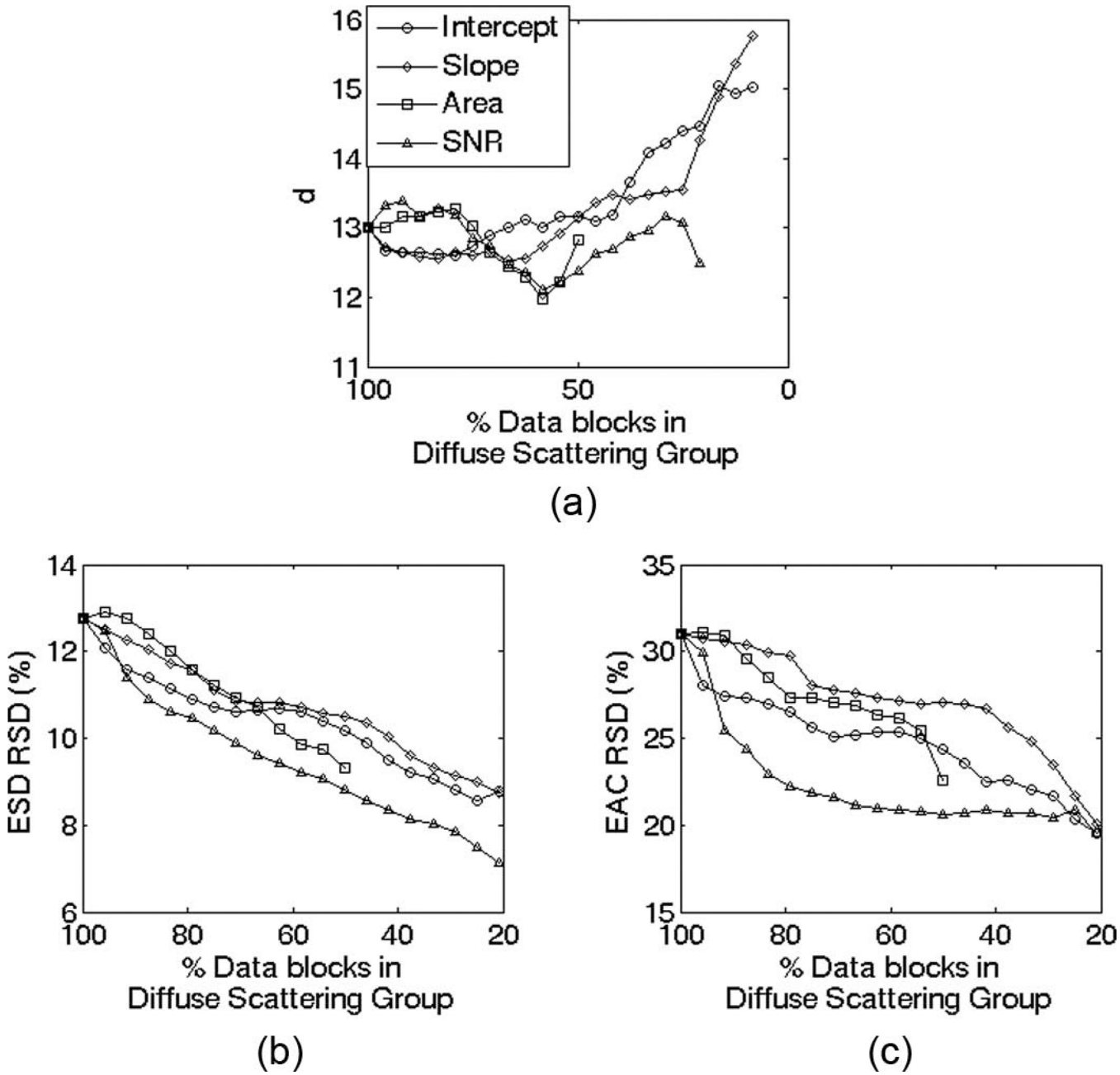


**Fig. 6.**

(a) Clustering distance averaged over the analyzed fibroadenoma slices and displayed as a function of the average percentage of data blocks sorted into the diffuse scattering group. (b) Effective scatterer diameter (ESD) relative standard deviation (RSD) and (c) effective acoustic concentration (EAC) RSD values averaged over the analyzed fibroadenoma slices and displayed as a function of the average percentage of data blocks sorted into the diffuse scattering group.

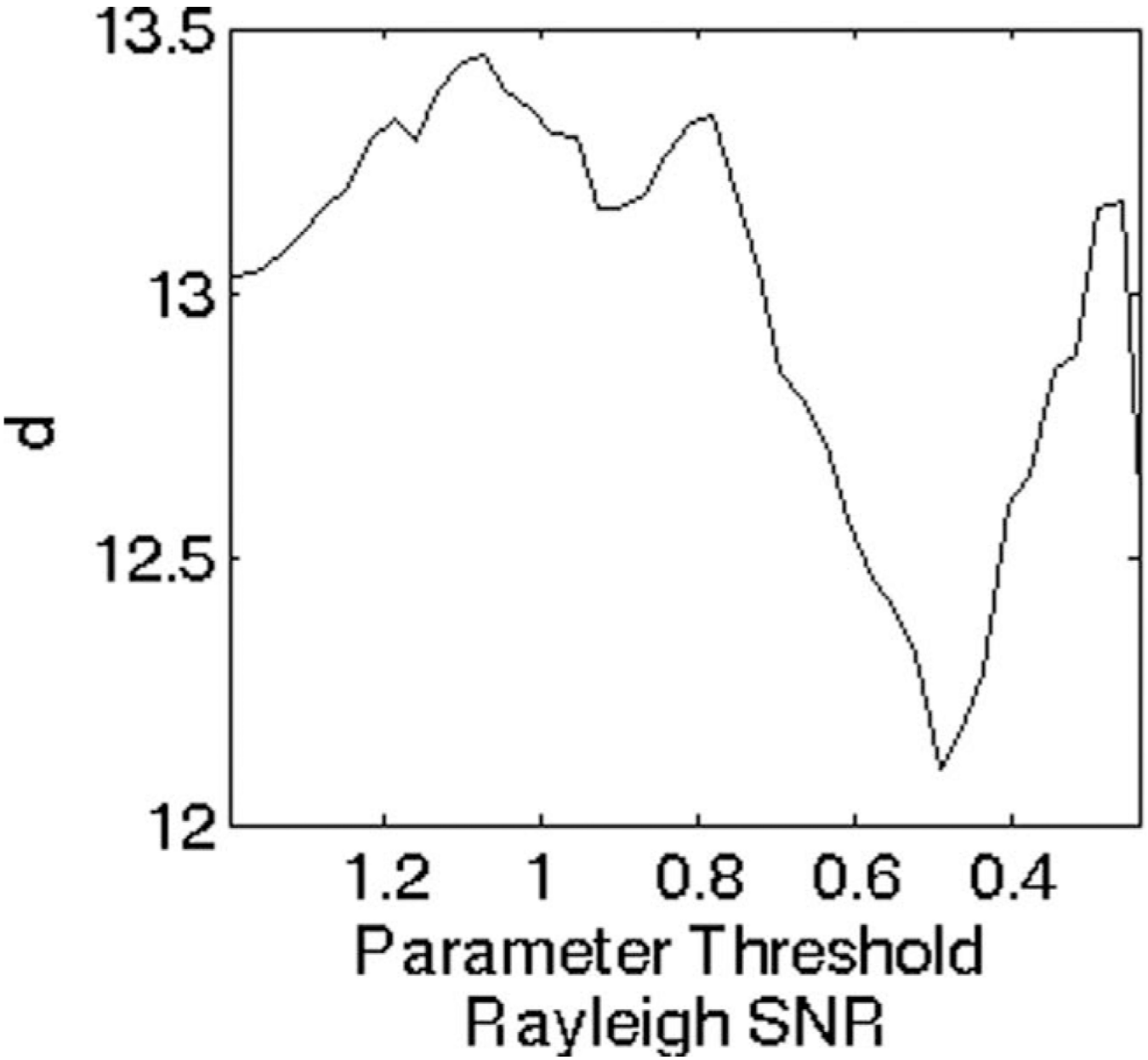


**Fig. 7.**
Clustering distance averaged over the analyzed fibroadenoma samples and displayed as a function of Rayleigh SNR sorting parameter.

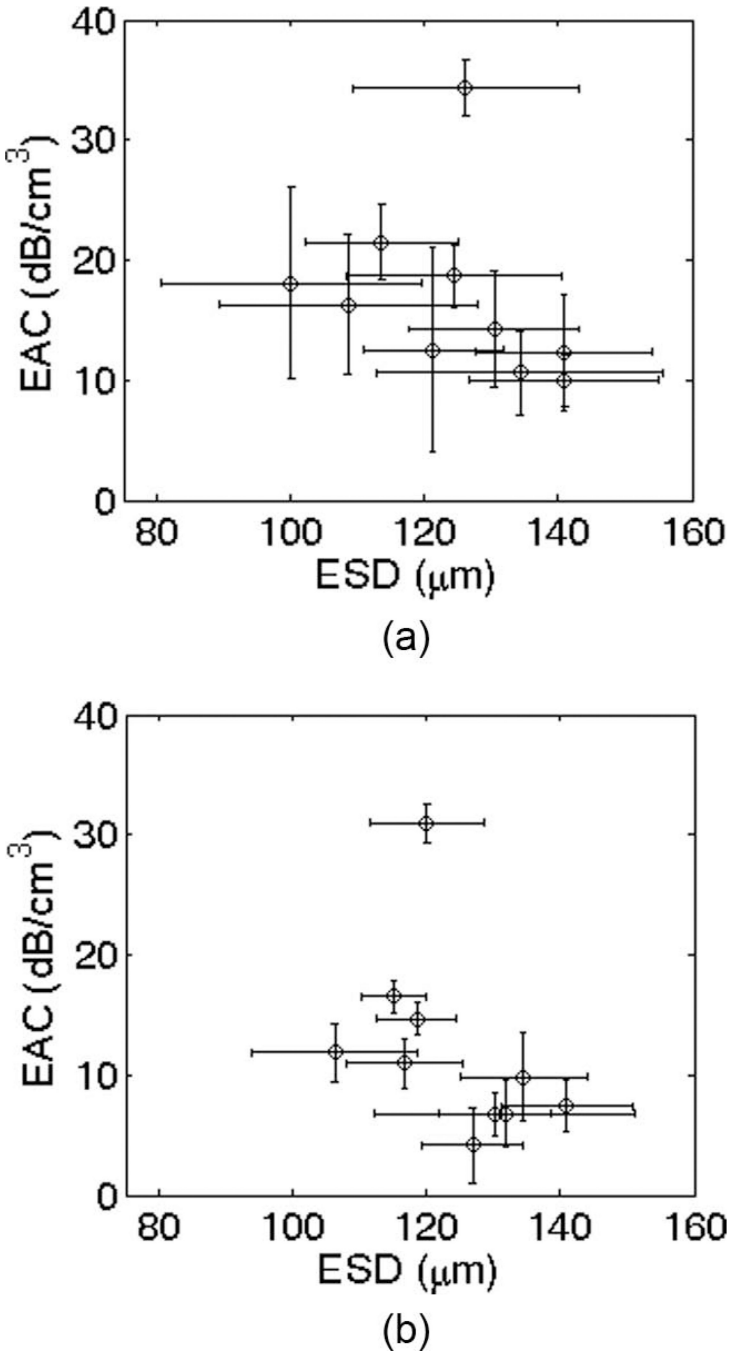


**Fig. 8.**

Fibroadenoma samples displayed according to their effective scatterer diameter (ESD) and effective acoustic concentration (EAC) mean values (a) when using all samples and (b) when using the Rayleigh SNR parameter as the sorting parameter with a threshold of 0.5. Error bars indicate one standard deviation. For the sample collection, the average fraction of data blocks sorted into the diffuse scattering group was 0.59 ± 0.09.

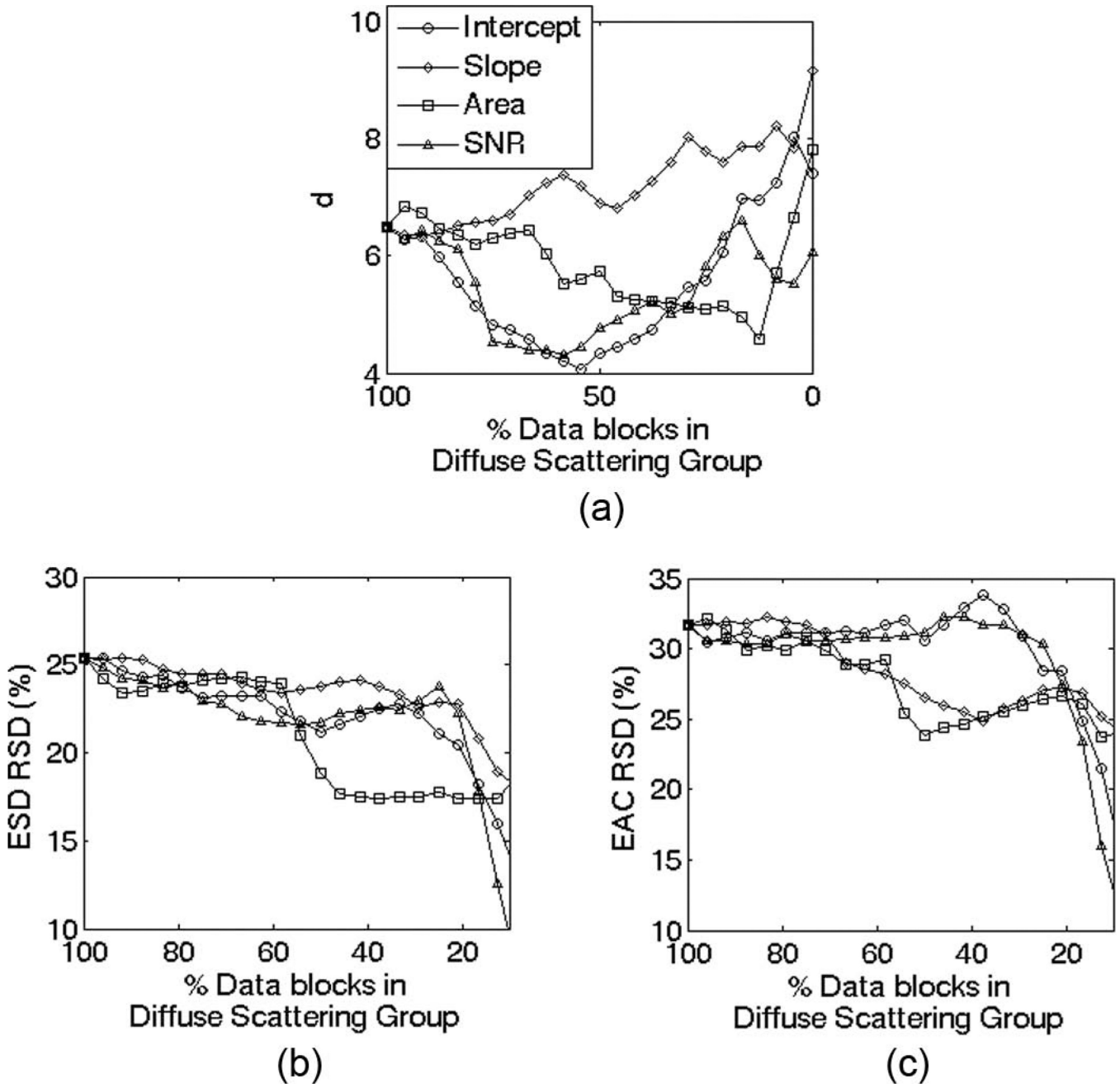


**Fig. 9.**

(a) Clustering distance averaged over the analyzed beef liver slices and displayed as a function of the average percentage of data blocks sorted into the diffuse scattering group. (b) Effective scatterer diameter (ESD) relative standard deviation (RSD) and (c) effective acoustic concentration (EAC) RSD values averaged over the analyzed beef liver slices and displayed as a function of the average percentage of data blocks sorted into the diffuse scattering group.

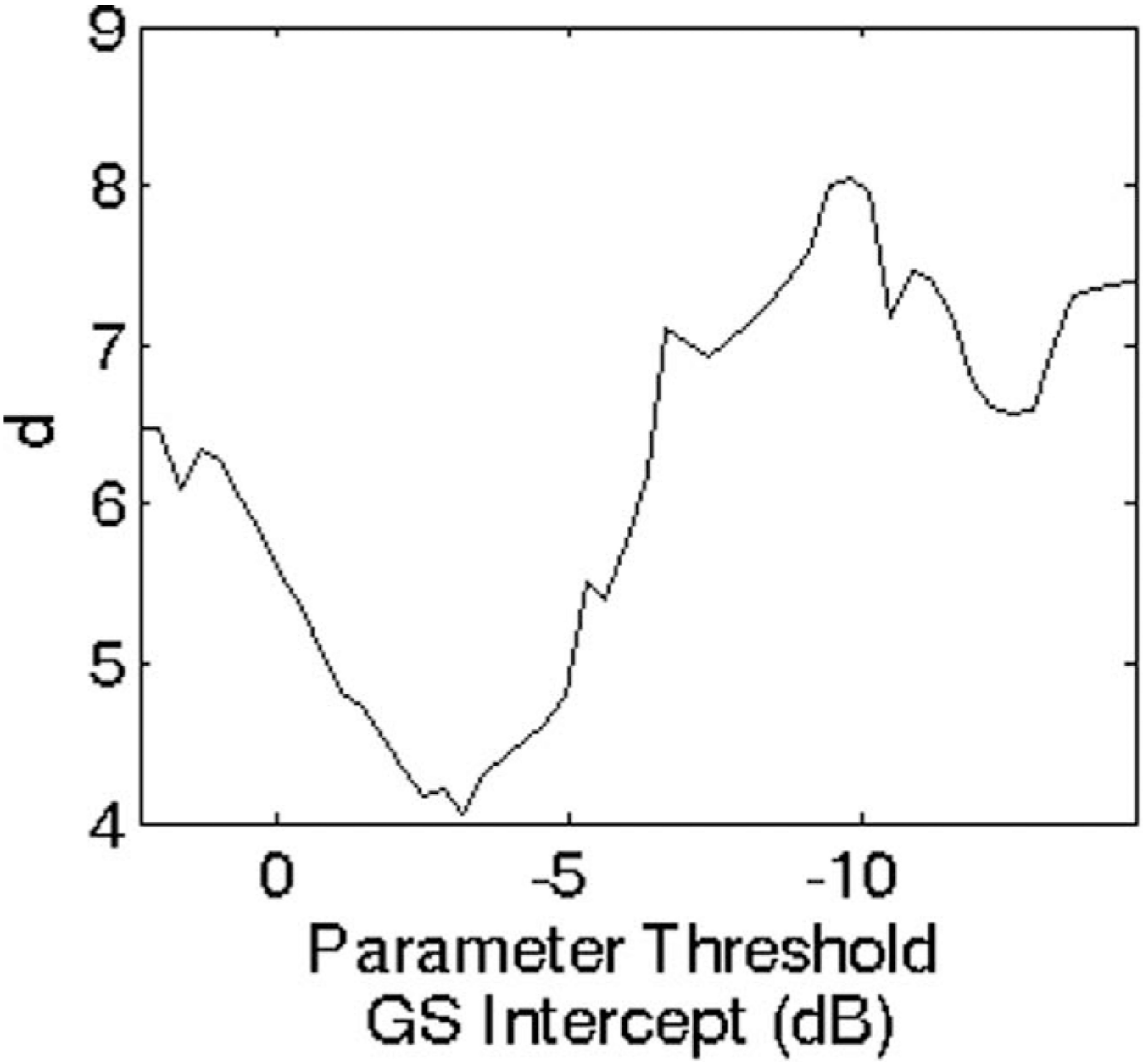


**Fig. 10.**
Clustering distance averaged over the analyzed beef liver slices and displayed as a function of generalized spectrum (GS) intercept sorting parameter.

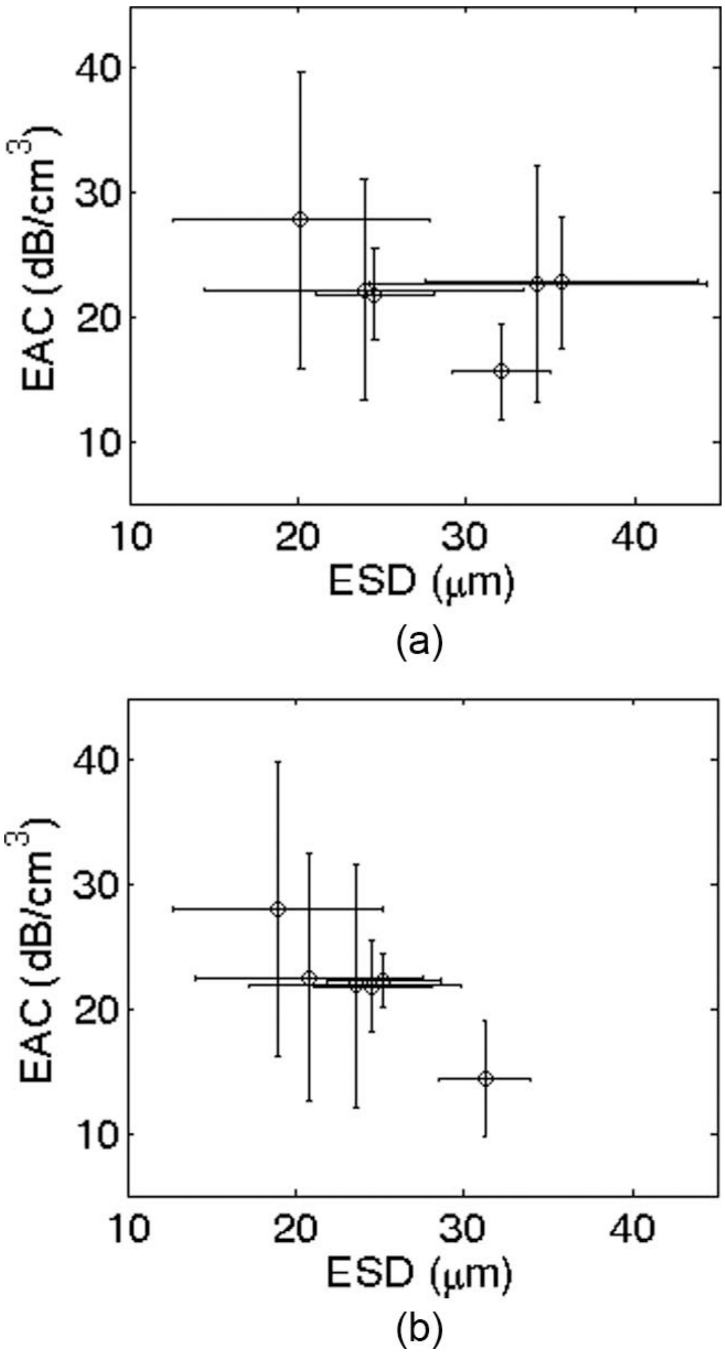


**Fig. 11.**

Beef liver samples displayed according to their effective scatterer diameter (ESD) and effective acoustic concentration (EAC) mean values (a) when using all samples and (b) when using the generalized spectrum (GS) intercept as a sorting parameter with a threshold of −3.2 dB. For the sample collection, the average fraction of data blocks sorted into the diffuse scattering group was 0.54 ± 0.34.